Finite-temperature properties of quasi-2D Bose-Einstein condensates

Kwangsik Nho and D. P. Landau
Center for Simulational Physics, University of Georgia, Athens, Georgia 30602
(Dated: February 6, 2008)

Using the finite-temperature path integral Monte Carlo method, we investigate dilute, trapped Bose gases in a quasi-two dimensional geometry. The quantum particles have short-range, s-wave interactions described by a hard-sphere potential whose core radius equals its corresponding scattering length. The effect of both the temperature and the interparticle interaction on the equilibrium properties such as the total energy, the density profile, and the superfluid fraction is discussed. We compare our accurate results with both the semi-classical approximation and the exact results of an ideal Bose gas. Our results show that for repulsive interactions, (i) the minimum value of the aspect ratio, where the system starts to behave quasi-two dimensionally, increases as the two-body interaction strength increases, (ii) the superfluid fraction for a quasi-2D Bose gas is distinctly different from that for both a quasi-1D Bose gas and a true 3D system, i.e., the superfluid fraction for a quasi-2D Bose gas decreases faster than that for a quasi-1D system and a true 3D system with increasing temperature, and shows a stronger dependence on the interaction strength, (iii) the superfluid fraction for a quasi-2D Bose gas lies well below the values calculated from the semi-classical approximation, and (iv) the Kosterlitz-Thouless transition temperature decreases as the strength of the interaction increases.

PACS numbers: 03.75.Hh, 03.75.Nt, 05.30.Jp, 02.70.Ss

The study of the effects of reduced dimensionality has attracted considerable interest in condensed matter physics and statistical physics, for example, quantum films of superfluid ^{4}He on surfaces, superfluid ^{4}He clusters, and superfluid ^{4}He confined in restricted geometries. Recently, the experimental realization of Bose-Einstein condensation (BEC) in dilute, trapped, and supercooled atomic vapors [1] and the additional ability to produce a low dimensional atomic gas trapped in an optical lattice have stimulated the investigation in a low dimensional system both theoretically [2, 3, 4, 5, 6] and experimentally [7, 8, 9, 10, 11, 12, 13, 14, 15, 16, 17, 18, 19, 20, 21, 22]. Dimensionally reduced systems have very different properties from their three dimensional (3D) counterparts [23, 24] due to the enhanced importance of phase fluctuations. For example, in a spatially homogeneous infinite system a one-dimensional (1D) Bose gas does not exhibit BEC, even at zero temperature; and in two dimensions (2D) BEC exists only at zero temperature. Nonetheless, a dilute two-dimensional Bose gas undergoes a superfluid phase transition at a finite critical temperature. Below the Kosterlitz-Thouless transition temperature [25], the gas is superfluid, and the superfluid phase is characterized by the presence of a quasicondensate, i.e., a condensate with only local phase coherence, since long wavelength phase fluctuations destroy long-range order.

Especially intriguing are two-dimensional Bose gases [26, 27, 28, 29, 30, 31, 32, 33, 36], and recently, experiments have entered regimes of BEC in 2D [9, 10, 11, 12, 13, 14]. In a spatially homogeneous two-dimensional system Safonov *et al.* [7] observed the first experimental evidence for a quasicondensate in 2D atomic hydrogen gas adsorbed on a superfluid ^{4}He surface. Furthermore, BEC in trapped gases is qualitatively different from BEC in a homogeneous potential. Lower dimensional trapped Bose gases have been realized with strong quantum confinement in one or more directions [30] (i) by gradually reducing atoms from a highly anisotropic trap to decrease the interaction energy [9, 10]; (ii) by gradually increasing the trap anisotropy while keeping the number of atoms fixed [11, 12]; and (iii) by using the periodic potential of a one-dimensional optical lattice [13, 14]. When the system is in a harmonic trap, the effect of the trap becomes more dramatic with lowering of dimensionality of the system; the external trapping potential limits the size of the atomic gas, and the density of states is modified. As a result, Bagnato and Kleppner [37] showed that an ideal 2D gas in a harmonic potential does exhibit a BEC phase at a finite temperature. Petrov *et al.* [38] showed that well below T_c the equilibrium state is a true condensate, whereas at intermediate temperatures a quasicondensate forms when local two-body interactions are included.

Theoretically, the ground-state properties of a trapped Bose gas in two dimensions have been studied recently using the Gross-Pitaevskii mean-field theory [34, 35], the leading quantum corrections to the Gross-Pitaevskii equation [27], and a variational model based on a Gaussian-parabolic trial wave function [30]. For the finite-temperature properties of a dilute Bose gas confined in a harmonic trap, the semiclassical approximation [39], a microscopic mean field theory that includes both density and phase fluctuations of the Bose gas [6], the Hartre-Fock-Bogoliubov formalism [26, 28, 29], and the scaling structure within diagrammatic perturbation theory [33] have been used.

However, many properties have yet to be investigated both experimentally and theoretically. Needless to say, a more thorough theoretical understanding is clearly desirable. At finite temperatures among the main problems

to be answered are the density profile as a function of temperature and the strength of the interparticle interaction, under what conditions the confinement gives a system with dimensionality 2, the superfluidity, and the effect of interactions on the critical temperature. In addition, as the role of correlations and of quantum fluctuations is enhanced in quasi-2D geometries, an appropriate theoretical description requires the more accurate many-body approach beyond the mean-field approximation for a more systematic investigation in a wider range of temperature and values of the scattering length.

In this paper we use a finite-temperature path-integral Monte Carlo (PIMC) method [40] to investigate the crossover from 3D to 2D for N particles, where the interparticle interaction is a purely repulsive hard-sphere potential of radius a_s, the s-wave scattering length. PIMC allows one to calculate accurate quantum mechanical expectation values of many-body system, the only input being the many-body potential. In particular, we demonstrate the influence of temperature T and interparticle interaction a_s on the equilibrium properties of ultracold atomic gases to calculate their energetics and structural properties in a highly anisotropic trap. Furthermore, we compare our accurate PIMC results with both the semiclassical approximation and the exact values for an ideal Bose gas, and we provide detailed predictions for comparison with future experiments.

We consider the following Hamiltonian for a system of N hard spheres

$$H = H_0 + \sum_{i>j}^{N} v(r_{ij}) \quad (1)$$

$$H_0 = -\frac{\hbar^2}{2m}\sum_{i=1}^{N}\nabla_i^2 + \frac{1}{2}m\sum_{i=1}^{N}(\omega_x^2 x_i^2 + \omega_y^2 y_i^2 + \omega_z^2 z_i^2),$$

where H_0 is the Hamiltonian for trapped ideal Bose gases and $v(r)$ is a two-body, symmetric hard-sphere potential defined by

$$v(r) = \begin{cases} +\infty & (r < a_s) \\ 0 & (r > a_s). \end{cases}$$

In order to investigate the crossover from 3D to 2D, we consider Bose gases under a cylindrically harmonic confinement ($\omega_x = \omega_y = \omega_\rho$ and $\omega_z = \lambda\omega_\rho$), where λ is the aspect ratio. Here we shall always be concerned with the properties of trapped Bose gases at finite temperatures with the number of particles N, the scattering length a_s, of the two-body interaction potential, and two characteristic lengths $a_z = \sqrt{\hbar/m\omega_z}$ and $a_\rho = \sqrt{\hbar/m\omega_\rho}$, describing the oscillation lengths in the transverse and the longitudinal directions, respectively. We gradually vary the axial trap frequency to increase the trap anisotropy and to enter the quasi-two-dimensional regime, where the particles obey 2D statistics but interact in the same way as in a three-dimensional system. As a result, the gas is confined by an extreme, pancake-shaped potential and has quasi-two-dimensional properties. Along the tightly confined axial direction the motion is frozen out, so that the condensate is in the harmonic oscillator ground state of an ideal gas, and the condensate width equals the harmonic oscillator length. The tight confining direction is characterized by the frequency ω_z and two weak confining directions by ω_ρ.

FIG. 1: The calculated density profiles $n(\rho)$, normalized such that $\int_0^\infty n(\rho)\rho d\rho = 1$ and $\rho = \sqrt{x^2+y^2}$, at $T = 0.4\ T_c$ for two different aspect ratios, i.e., $\lambda = 10$ and $\lambda = 100$. We used three different scattering lengths $a_s = 0$ (solid lines), $a_s = a_{Rb}$ (dotted lines), and $a_s = 10a_{Rb}$ (dashed lines). The inset shows the expectation value of ρ in unit of a_ρ as a function of λ for $a_s = 0$ (triangles), $a_s = a_{Rb}$ (diamonds), and $a_s = 10a_{Rb}$ (circles). In all figures, when statistical errors cannot be seen on the scale of the figure, the error bars are smaller than the symbol sizes. The expectation value of ρ clearly depends on both the scattering length a_s and the aspect ratio λ. The dependence on a_s becomes increasingly large as λ increases.

In this study, we typically use N=27 hard spheres because the permutation sampling in PIMC is efficient if $N = \mathrm{L}^3$, where L is an integer [41], and the next largest number that satisfies this criterion would have required an excessive amount of cpu time. There is a finite-size effect in the density profile and the total energy; however, the superfluid fraction shows no dependence upon N within the statistical error of the data. Experimentally, in an optical lattice, one can control and reduce the number of particle in each BEC [14, 42]. Consequently, it will be possible to compare the effects predicted here for small numbers of atoms with experimental data directly. We also use several trap aspect ratios $1 \le \lambda = \omega_z/\omega_\rho \le 300$ and a wide temperature range, i.e., $0.1 \le T/T_c \le 1.4$, wheret T_c is the transition temperature for an ideal Bose gas of N atoms in a trap (see, e.g., Eq. (19) of Ref. [2]). Due to the finite-size corrections, the critical temperature T_c depends on both the number of atoms N and trapping frequencies, ω_ρ and ω_z. For a repulsively interacting trapped Bose gas, T_c is lowered compared to the trapped

FIG. 2: The calculated density profiles $n(\rho)$ at the aspect ratio $\lambda = 100$ for two different temperatures, i.e., $T/T_c = 0.2$ and $T/T_c = 1.2$ using three different scattering lengths $a_s = 0$, $a_s = a_{Rb}$, and $a_s = 10a_{Rb}$. The inset shows the dependence of the expectation values of ρ on the temperature T/T_c. The arrow on the y-axis indicates the expectation value of ρ at $T = 0$, $< \rho > = 0.886\ a_\rho$. As the temperature increases, the density profiles $n(\rho)$ expand along the ρ axis and the effect of the interaction strength decreases.

ideal Bose gas as a result of interaction, in contrast to an uniform Bose gas in the dilute range, where the critical temperature is increased above the ideal Bose gas value by interaction. Here, the length unit is a_ρ, where $a_\rho = \sqrt{\hbar/m\omega_\rho}$, and energies are measured in units of $\hbar\omega_\rho$.

In addition, we assume that the s-wave scattering length a_{Rb} of ^{87}Rb is 100 times the Bohr radius, i.e., $a_{Rb} = 0.00433\ a_\rho$. PIMC procedure used here is based on methods described in our previous work [43].

We first discuss the density profiles of $N = 27$ hard spheres at $T = 0.4\ T_c$ as a function of λ, $1 \le \lambda \le 300$. Figure 1 shows the calculated density profiles $n(\rho)$ as a function of ρ, normalized such that $\int_0^\infty n(\rho)\rho d\rho = 1$ and $\rho = \sqrt{x^2 + y^2}$, for two different aspect ratios, i.e., $\lambda = 10$ and $\lambda = 100$. To study the effect of the interaction strength, we used three different scattering lengths $a_s = 0$ (solid lines), $a_s = a_{Rb}$ (dotted lines), and $a_s = 10a_{Rb}$ (dashed lines). Clearly, the total density profile along the ρ coordinate spreads out in the trap as both a_s and λ increases, i.e., the density at the center of the trap decreases with increasing λ and a_s as expected. In particular, the density profile $n(\rho)$ depends strongly on the interaction strength a_s for $\lambda \ge 10$ and changes dramatically as a function of the aspect ratio λ. However, for $\lambda = 1$ (a spherically symmetric harmonic trap), the density profile $n(\rho)$ for $a_s = a_{Rb}$ approaches that of the non-interacting gas (see the inset of Fig. 1).

The inset of Fig. 1 shows the expectation value of ρ in unit of a_ρ as a function of λ for $a_s = 0$ (triangles), $a_s = a_{Rb}$ (diamonds), and $a_s = 10a_{Rb}$ (circles). In all figures, when statistical errors cannot be seen on the scale of the figure, the error bars are smaller than the symbol sizes. The expectation value of ρ clearly depends on both the scattering length a_s and the aspect ratio λ. The dependence on a_s becomes increasingly large as λ increases, which suggests that the repulsion between the atoms spreads the atoms in the trap as a result of interaction.

Next, we further examine the condition to achieve a quasi-2D Bose gas using the density profiles $n(z)$ along the axial direction as a function of z, normalized such that $\int_{-\infty}^{\infty} n(z)dz = 1$, and the expectation value of $|z|$. In the quasi-2D regime, along the z direction the gas at finite temperatures has the characteristics of an ideal non-interacting gas at $T = 0$. Thus, the density profile $n(z)$ becomes identical to that of an ideal gas,

$$n(z) = \frac{1}{\sqrt{\pi}a_z} \exp[-(z/a_z)^2]. \quad (2)$$

From Eq. (2), the expectation value of $|z|$ is $0.564\ a_z$ for an ideal Bose gas at $T = 0$.

Our calculated expectation values of $|z|$ for $a_s = a_{Rb}$ at $T = 0.4T_c$ approach the ground state value ($T = 0$) as the aspect ratio λ increases. Our calculated density profile $n(z)$ for $a_s = a_{Rb}$ at $T = 0.4T_c$ and that for an ideal gas (Eq. (2)) are indistinguishable for $\lambda \ge 40$. This suggests that the motion along the z coordinate is indeed frozen out as λ approaches large values since the energy of the axial excitations increases with increasing λ and it is not easy for particles to go to the excited states for large values of λ. For repulsive interactions, the minimum value of λ, where the system starts to enter a quasi-2D regime, increases as the interaction strength increases.

To see the effect of the temperature T, we also calculated the density profiles $n(\rho)$ and $n(z)$ and the expectation values of ρ and $|z|$ as a function of the scaled temperature T/T_c for the aspect ratio $\lambda = 100$ and $N = 27$.

Figure 2 shows the calculated density profiles $n(\rho)$ as a function of ρ, for two different temperatures, i.e., $T/T_c = 0.2$ and $T/T_c = 1.2$ using three different scattering lengths $a_s = 0$, $a_s = a_{Rb}$, and $a_s = 10a_{Rb}$ (using the same symbols as in Fig. 1). As the temperature increases, the density profiles $n(\rho)$ expand along the ρ axis and the effect of the interaction decreases.

The inset of Fig. 2 shows the dependence of the expectation values of ρ on the temperature T/T_c. At very low temperatures, our calculated expectation values of ρ for $a_s = 0$ approach the ground state value, i.e., $\langle\rho\rangle = 0.886\ a_\rho$ (see the arrow on the y-axis). As the temperature increases, the expectation values of ρ increase, but the effect of the interaction decreases. The expectation values of ρ for $a_s = 0$ and $a_s = a_{Rb}$ are the same within errorbars at high temperatures. However, the expectation values of ρ for $a_s = 10a_{Rb}$ are still larger than those for $a_s = 0$ even at high temperatures.

FIG. 3: The calculated PIMC total energies per particle E/N in units of $\hbar\omega_\rho$ as a function of the scaled temperature T/T_c for $N = 27$ and $\lambda = 100$. We use three different interaction strengths $a_s = 0$, $a_s = a_{Rb}$, and $a_s = 10a_{Rb}$. In the figure, we subtract $E_0^z = \hbar\omega_z/2 = 50\ \hbar\omega_\rho$, the ground energy of an ideal Bose gas in the tight confinement direction, from our PIMC total energy. The arrow on the y-axis indicates the ideal gas energy per particle in the ρ direction, $\hbar\omega_\rho$, at $T = 0$.

FIG. 4: The superfluid fraction along the axis of rotation z for $T/T_c = 0.4$ and N =27 as a function of the aspect ratio λ calculated using the PIMC method. In this calculation we have used three different interaction strengths $a_s = 0$, $a_s = a_{Rb}$, and $a_s = 10a_{Rb}$. At the aspect ratios $\lambda < 100$, the superfluid fraction decreases as the aspect ratio increases. However, the superfluid fractions do not depend on the aspect ratio, to within error bars, for aspect ratios $\lambda \geq 100$.

In contrast to the expectation value of ρ, the expectation value of $|z|$ for $\lambda = 100$ is nearly constant for $T \leq 1.4T_c$, the whole temperature range used here, and is the same as that for the ground state of an ideal Bose gas. Thus, the motion in the axial direction is largely frozen out and the system behaves quasi-two dimensionally at those temperatures. This demonstrates clearly that for the axial axis the system at finite temperatures behaves like an ideal gas at $T = 0$.

Figure 3 shows our calculated PIMC total energies per particle E/N in units of $\hbar\omega_\rho$ as a function of the scaled temperature T/T_c for $N = 27$ and $\lambda = 100$. We used three different interaction strengths $a_s = 0$, $a_s = a_{Rb}$, and $a_s = 10a_{Rb}$. For large anisotropies and small atom numbers, the total energy per particle tends towards $\hbar\omega_z/2$, the ground energy of an ideal Bose gas in the tight confinement direction. As shown above, the motion along the z direction is indeed frozen out at $\lambda = 100$ for all temperature range used in this calculation $0.1 \leq T/T_c \leq 1.4$, i.e., the total energy per particle in the tight confinement direction equals that for an ideal Bose gas in one dimension, $\hbar\omega_z/2 = 50\ \hbar\omega_\rho$. In the figure, we subtracted $E_0^z = \hbar\omega_z/2 = 50\ \hbar\omega_\rho$ from our PIMC total energy per particle E/N to interpret our results.

Our calculated PIMC energies per particle for $a = 0$ in the ρ direction, E/N - E_0^z, only approach the ideal gas energy per particle in the ρ direction, $\hbar\omega_\rho$, with decreasing temperature as expected (see the arrow on the y-axis). Above T_c the total energies per particle for $a = 0$ increase linearly with increasing temperature. However, below T_c the total energy per particle decreases non-linearly with decreasing temperature, as expected theoretically [2]. The specific heat can be calculated by differentiating the total energy per particle with respect to the temperature to locate the critical temperature T_c, where the specific heat has a peak in plotting the values of the specific heat as a function of temperature. In the present calculation, however, it is not easy to see a peak due to the finite size of our system and large error bars. The scaled energies for $a = 10a_{Rb}$ lie well above the non-interacting curve both below and above T_c. The difference in the total energy per particle between for an ideal Bose gas and for a hard-sphere gas is visible at the low temperatures, and the clear difference increases as T decreases because of the short-range structure of the hard-sphere potential, i.e., the comparison between the total energy for an ideal Bose gas and that for a hard-sphere gas shows that the scaled energies per particle clearly shows the effect of the interaction strength.

Finally, we calculated the superfluid fraction from PIMC data using the projected area [43], not using the winding number because we used open boundary conditions along all three axies. The superfluid fraction depends on the rotation axis for the anisotropic trap. In particular, we calculated the superfluid fraction with respect to the symmetry axis, i.e., the z axis. Figure 4 shows the superfluid fraction as a function of the aspect ratio λ calculated using the PIMC method. In this calculation we used $T/T_c = 0.4$, N =27, and three different interaction strengths $a_s = 0$, $a_s = a_{Rb}$, and $a_s = 10a_{Rb}$

FIG. 5: The calculated superfluid fractions along the z axis at the aspect ratio λ =100 and N = 27 for three different interaction strengths $a_s = 0$ (circles), $a_s = a_{Rb}$ (diamonds), and $a_s = 10a_{Rb}$ (triangles) as a function of the scaled temperature T/T_c. The inset shows the superfluid fraction along the z axis for a quasi-1D Bose gas (using the same symbols as in Fig. 3). Solid lines show the theoretical superfluid fraction along the z axis for an ideal Bose gas calculated from Eq. (3).

(using the same symbols as in Fig. 3). For aspect ratios $\lambda < 100$, the superfluid fraction decreases as the aspect ratio increases. However, the superfluid fractions do not depend on the aspect ratio within error bars for aspect ratios $\lambda \geq 100$. Figure 4 also shows that the superfluid fraction decreases gradually as both the two-body interaction strength and the aspect ratio increase.

In Fig. 5 we present our calculated superfluid fractions for the aspect ratio λ =100 as a function of the scaled temperature T/T_c. In the calculation, we used N= 27 and three different interacting strengths $a_s = 0$, $a_s = a_{Rb}$, and $a_s = 10a_{Rb}$ (using the same symbols as in Fig. 3). The superfluid fraction decreases from unity at very low temperatures and becomes zero above the critical temperature T_c as the temperature increases. The superfluid fraction has a small value at the same temperature for an interacting Bose gas compared to a non-interacting Bose gas, which shows that the critical temperature for a repulsively interacting Bose gas is lowered compared to the ideal Bose gas as a result of interaction. The inset of Fig. 5 shows the superfluid fraction for a quasi-1D Bose gas [44].

The superfluid fraction for a quasi-1D Bose gas decreases much more slowly than that for a quasi-2D Bose gas with increasing temperature. For example, at the scaled temperature, $T/T_c = 1$, the superfluid fraction for a quasi-1D system is significantly larger, about 0.65, compared to that for a quasi-2D gas, about 0.01. However, the superfluid fraction for a quasi-2D gas shows a clear dependence on the interaction strength whereas a quasi-1D gas shows no noticeable dependence.

In order to compare our calculated PIMC data for the superfluid fraction with the theoretical value of an ideal gas [39], we calculated the theoretical superfluid fraction for an ideal Bose gas using Eq. (14) of Ref. [39]. The superfluid fraction N_s/N is 1 - Θ/Θ_{rig} [40], where Θ is the quantum mechanical moment of inertia and Θ_{rig} is the classical moment of inertia. In our case, we used the T_c with the first finite-size correction term (see, e.g., Eq. (19) of Ref. [2]). For this, we modified Eq. (14) of Ref. [39] by simply rewriting Eq. (14) of Ref. [39] using Eqs. (8) and (9) of Ref. [39] to yield [44]

$$\left(\frac{N_s}{N}\right)_z = \frac{1-(T/T_c)^3}{1-(T/T_c)^3+1.801(T/T_c)^4(k_BT_c/\hbar\omega_\rho)}. \quad (3)$$

In order to derive Eq. (14) of Ref. [39], Stringari used the semiclassical approximation in the so-called macroscopic limit. The solid lines in Fig. 5 and in the inset of Fig. 5 show the resulting approximate superfluid fraction. For a quasi-1D Bose gas, the theoretical values agree well with PIMC data below $T/T_c \leq 0.6$ and after $T/T_c = 0.6$ the difference between the theoretical values and PIMC data gets larger as the scaled temperature increases. However, for a quasi-2D system, the values calculated from Eq. (3) lie well above our calculated PIMC data below T_c.

In summary, using a finite-temperature path integral Monte Carlo technique we have investigated a trapped Bose gas in quasi-two dimensions interacting via a hard sphere potential whose core radius equals its corresponding scattering length. In order to enter a quasi-2D regime, we have changed the axial trapping frequency ω_z. We have presented and analyzed our accurate PIMC results such as the total energy, the density profile, and the superfluid fraction as a function of temperature T/T_c at various values of the strength of the interaction and the aspect ratio λ. We have compared our results with both the semi-classical approximation and the ideal Bose gas. We find that for repulsive interactions, the minimum value of the aspect ratio λ, where the system start to behave quasi-two dimensionally, increases as the interaction strength increases. In addition, for N = 27 and λ = 100, the motion along the axial direction is indeed frozen out for all temperature range used in this paper 0.1 $\leq T/T_c \leq$ 1.4 and the density profile $n(z)$ becomes identical to that of an ideal gas. Specifically, we have calculated the superfluid fraction using the projected area and have compared the superfluid fraction for a quasi-2D system to that for a quasi-1D Bose gas. The superfluid fraction for a quasi-2D Bose gas is distinctly different from that for both a quasi-1D Bose gas and a true 3D system, i.e., the superfluid fraction for a quasi-2D Bose gas decreases faster than that for a quasi-1D system and a true 3D system with increasing temperature, and shows a stronger dependence on the interaction strength. In addition, the superfluid fraction for a quasi-2D Bose gas lie well below the values calculated from the semi-classical approxima-

tion and the Kosterlitz-Thouless transition temperature decreases as the strength of the interaction increases.

Acknowledgments

We are greatly indebted to P. Stancil and C. D. Fertig for their critical reading of the manuscript and illuminating comments. This work was partially supported by NASA grant No. NNC04GB24G.

[1] M. H. Anderson, J. R. Ensher, M. R. Matthews, C. E. Wieman, and E. A. Cornell, Science **269**, 198 (1995); K. B. Davis, M. -O. Mewes, M. R. Andrews, N. J. van Druten, D. S. Durfee, D. M. Kurn, and W. Ketterle, Phys. Rev. Lett. **75**, 3969 (1995); C. C. Bradley, C. A. Sackett, and R. G. Hulet, ibid. **78**, 985 (1997).

[2] For a general review of BEC, see F. Dalfovo, S. Giorgini, L. P. Pitaevskii, and S. Stringari, Rev. Mod. Phys. **71**, 463 (1999).

[3] G. E. Astrakharchik, D. Blume, S. Giorgini, and B. E. Granger, Phys. Rev. Lett. **92**, 030402 (2004).

[4] E. H. Lieb, R. Seiringer, and J. Yngvason, Phys. Rev. Lett. **91**, 150401 (2003).

[5] P. Ohberg and L. Santos, Phys. Rev. Lett. **89**, 240402 (2004).

[6] J. O. Andersen, U. Al Khawaja, and H. T. C. Stoof, Phys. Rev. Lett. **88**, 070407 (2002).

[7] A. I. Safonov, S. A. Vasilyev, I. S. Yasnikov, I. I. Lukashevich, and S. Jaakkola, Phys. Rev. Lett. **81**, 4545 (1998).

[8] F. Schreck, L. Khaykovich, K. L. Corwin, G. Ferrari, T. Bourdel, J. Cubizolles, and C. Salomon, Phys. Rev. Lett. **87**, 080403 (2001).

[9] A. Görlitz, J. M. Vogels, A. E. Leanhardt, C. Raman, T. L. Gustavson, J. R. Abo-Shaeer, A. P. Chikkatur, S. Gupta, S. Inouye, T. Rosenband, and W. Ketterle, Phys. Rev. Lett. **87**, 130402 (2001).

[10] D. Rychtarik, B. Engeser, H. -C. Nagerl, and R. Grimm, Phys. Rev. Lett. **92**, 173003 (2004).

[11] T. P. Meyrath, F. Schreck, J. L. Hanssen, C. -S. Chuu, and M. G. Raizen, Phys. Rev. A **71**, 041604(R) 2005.

[12] N. L. Smith, W. H. Heathcote, G. Hechenblaikner, E. Nugent, and C. J. Foot, J. Phys. B **38**, 223 (2005).

[13] S. Stock, Z. Hadzibabic, B. Battelier, M. Cheneau, and J. Dalibard, cond-mat/0506559; Z. Hadzibabic, S. Stock, B. Battelier, V. Bretin, and J. Dalibard, Phys. Rev. Lett. **93**, 180403 (2004).

[14] I. B. Spielman, P. R. Johnson, J. H. Huckans, C. D. Fertig, S. L. Rolston, W. D. Phillips, and J. V. Porto, cond-mat/0509079.

[15] C. D. Fertig, K. M. O'Hara, J. H. Huckans, S. L. Rolston, W. D. Phillips, and J. V. Porto, Phys. Rev. Lett. **94**, 120403 (2005).

[16] C. Schori, T. Stoferle, H. Moritz, M. Kohl, and T. Esslinger, Phys. Rev. Lett. **93**, 240402 (2004).

[17] Z. Hadzibabic, S. Stock, B. Battelier, V. Bretin, and J. Dalibard, Phys. Rev. Lett. **93**, 180403 (2004).

[18] B. L. Tolra, K. M. O'Hara, J. H. Huckans, W. D. Phillips, S. L. Rolston, and J. V. Porto, Phys. Rev. Lett. **92**, 190401 (2004).

[19] T. Stoferle, H. Moritz, C. Schori, M. Kohl, and T. Esslinger, Phys. Rev. Lett. **92**, 130403 (2004).

[20] H. Moritz, T. Stoferle, M. Kohl, and T. Esslinger, Phys. Rev. Lett. **91**, 250402 (2003).

[21] B. Parades, A. Widera, V. Murg, O. Mandel, S. Folling, I. Cirac, G. V. Shlyapnikov, T. W. Hansch, and I. Bloch, Nature (London) **429**, 277 (2004).

[22] T. Kinoshita, T. Wenger, and D. S. Weiss, Science **305**, 1125 (2004).

[23] N. D. Mermin and H. Wagner, Phys. Rev. Lett. **22**, 1133 (1966).

[24] P. C. Hohenberg, Phys. Rev. **158**, 383 (1967).

[25] V. L. Berezinskii, Sov. Phys. JETP **32**, 493 (1971); **34**, 610 (1972);J. M. Kosterlitz and D. J. Thouless, J. Phys. C **6**, 1181 (1973);J. M. Kosterlitz, J. Phys. C **7**, 1047 (1974).

[26] J. P. Ternandez and W. J. Mullin, cond-mat/0203175.

[27] J. O. Andersen and H. Haugerud, Phys. Rev. A **65**, 033615 (2002).

[28] C. Gies, B. P. van Zyl, S. A. Morgan, and D. A. W. Hutchinson, Phys. Rev. A **69**, 023616 (2004).

[29] C. Gies and D. A. W. Hutchinson, Phys. Rev. A **70**, 043606 (2004).

[30] G. Hechenblaikner, J. M. Krueger, and C. J. Foot, Phys. Rev. A **71**, 013604 (2005).

[31] F. Mazzanti, A. Polls, and A. Fabrocini, Phys. Rev. A **71**, 033615 (2005).

[32] W. Purwanto and S. Zhang, cond-mat/0506219.

[33] M. Holzmann, G. Baym, J. -P. Blaizot, and F. Laloë, cond-mat/0508131.

[34] T. Haugset and H. Haugerud, Phys. Rev. A **57**, 3809 (1998).

[35] T. H. Hansson, J. M. Leinaas, and S. Viefers, Phys. Rev. Lett. **86**, 2930 (2001).

[36] For a general review of BEC in 2D, see A. Posazhennikova, cond-mat/0506034.

[37] V. Bagnato and D. Kleppner, Phys. Rev. A **44**, 7439 (1991).

[38] D. S. Petrov, M. Holzmann, and G. V. Shlyapnikov, Phys. Rev. Lett. **84**, 2551 (2000).

[39] S. Stringari, Phys. Rev. Lett. **76**, 1405 (1996).

[40] D. M. Ceperley, Rev. Mod. Phys. **67**, 279 (1995).

[41] The cyclic permutation of L atoms is accomplished via a random walk through permutation space. It is more efficient to use $L < N$; however, it is not easy to determine how big L should be, although our experience suggests that $L=(N)^{1/3}$ works well.

[42] M. Greiner, O. Mandel, T. Esslinger, T. W. Hansch, and I. Bloch, Nature (London) **415**, 39 (2002).

[43] K. Nho and D. P. Landau, Phys. Rev. A **70**, 053614 (2004); K. Nho and D. P. Landau, Phys. Rev. A **72**, 023615 (2005).

[44] K. Nho and D. Blume, Phys. Rev. Lett. **95**, 193601

(2005).

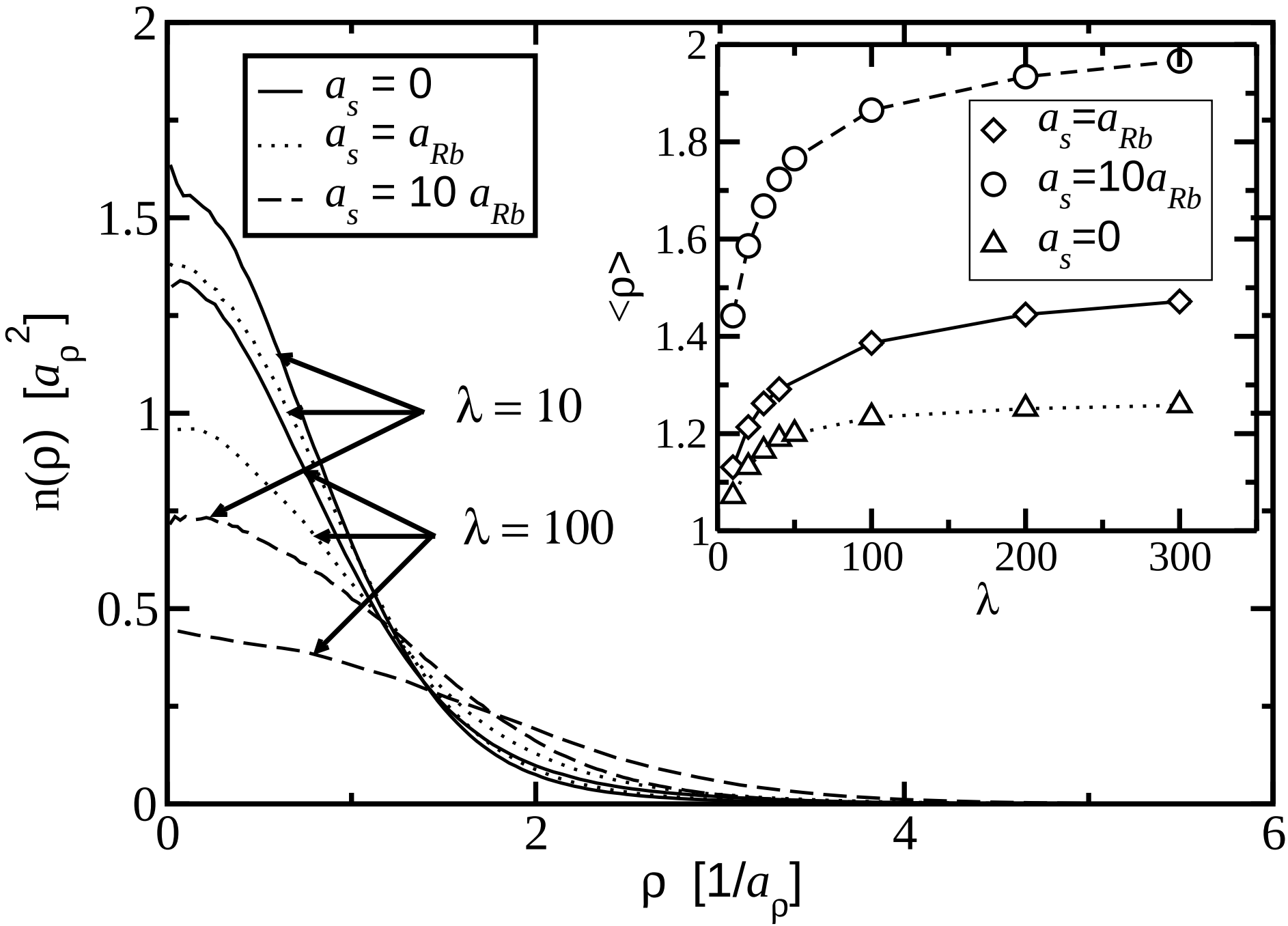
$a_s = 0$
$a_s = a_{Rb}$
$a_s = 10\ a_{Rb}$
$\lambda = 10$
$\lambda = 100$
n(ρ) [a_ρ^2]
ρ [1/a_ρ]
a_s=a_{Rb}
a_s=10a_{Rb}
a_s=0
<ρ>
λ

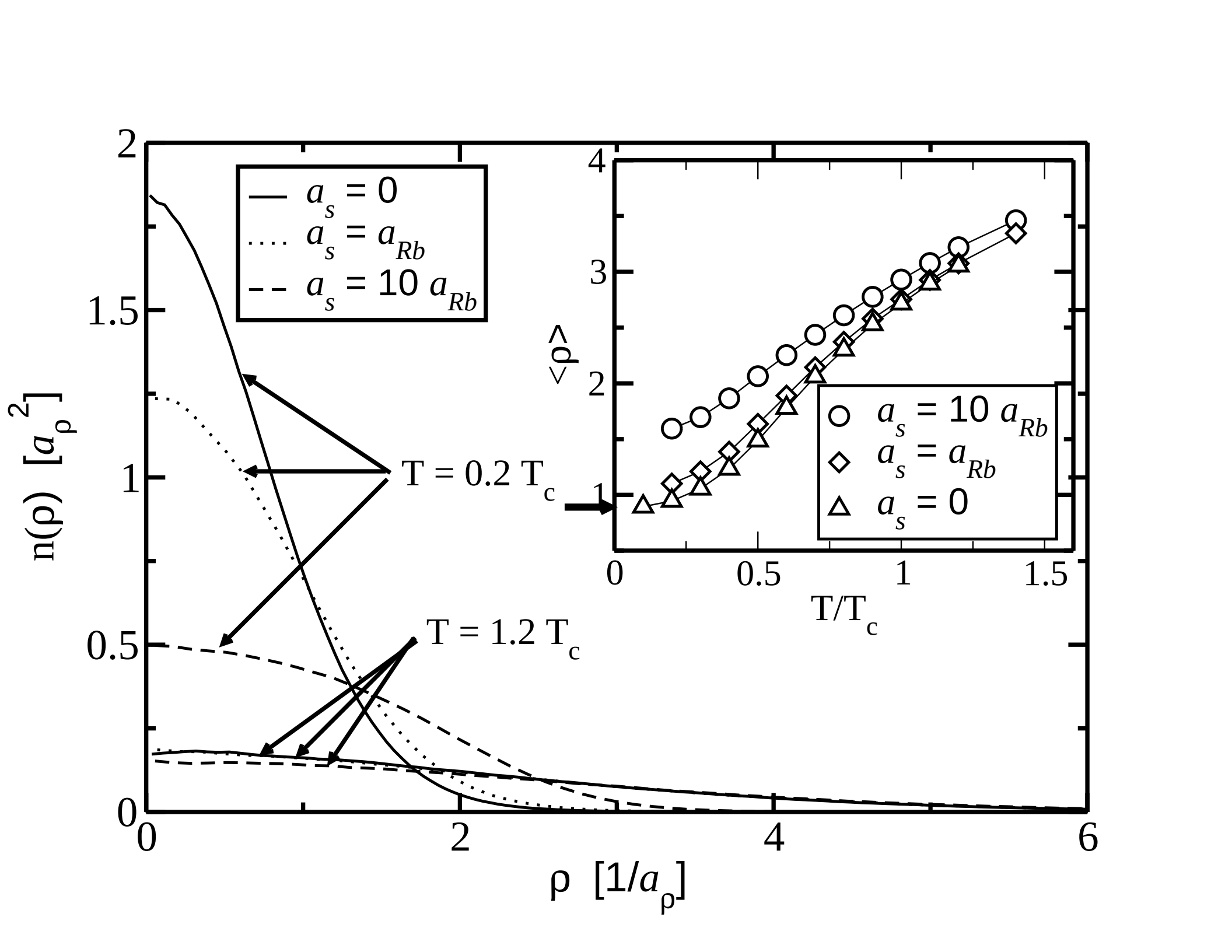
$a_s = 0$
$a_s = a_{Rb}$
$a_s = 10\ a_{Rb}$
T = 0.2 T_c
T = 1.2 T_c
n(ρ) [a_ρ^2]
ρ [1/a_ρ]
$\langle\rho\rangle$
T/T_c
$a_s = 10\ a_{Rb}$
$a_s = a_{Rb}$
$a_s = 0$

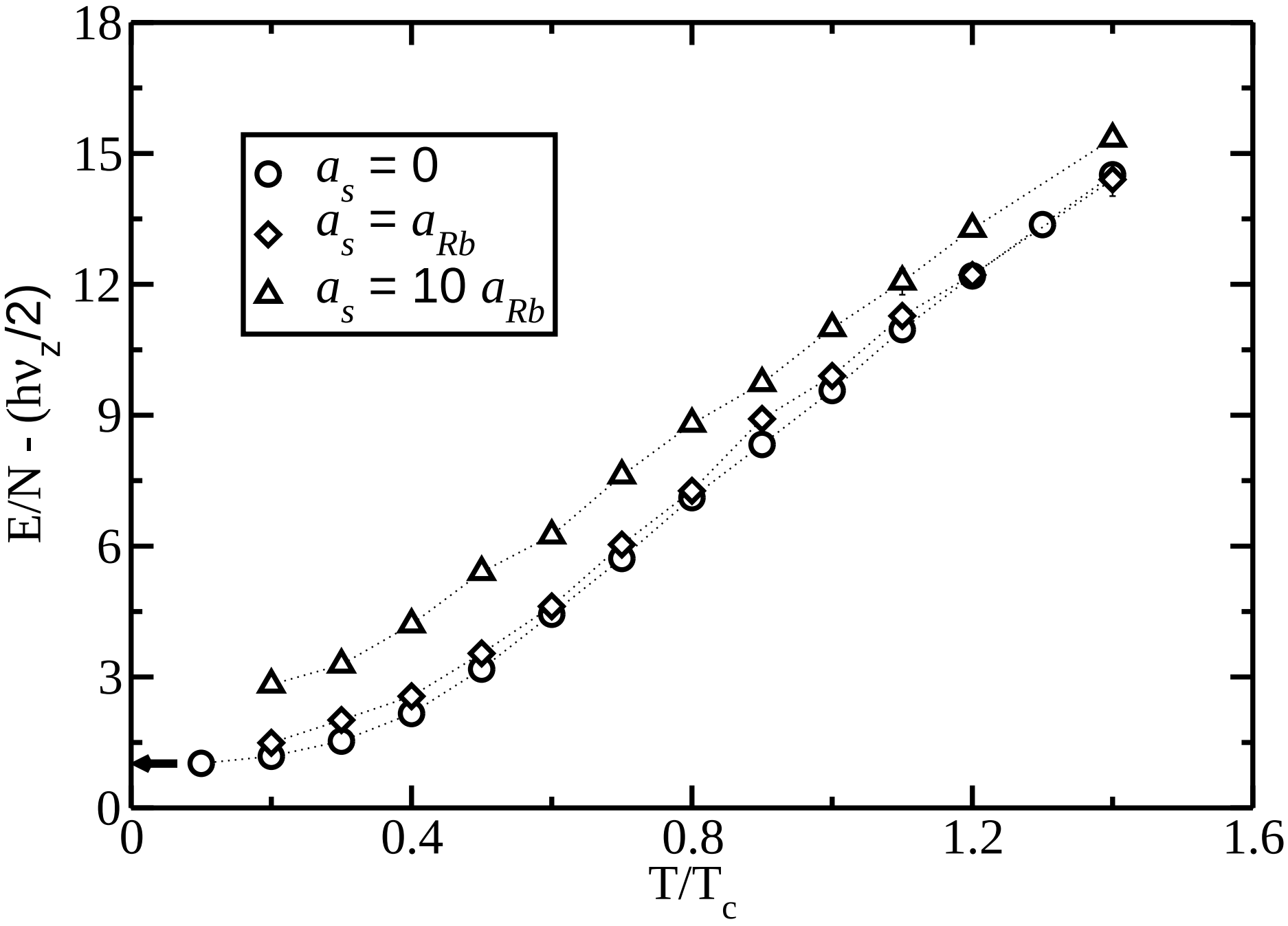
18
15
12
9
6
3
0
0
0.4
0.8
1.2
1.6
E/N - (hν_z/2)
T/T_c
a_s = 0
a_s = a_Rb
a_s = 10 a_Rb

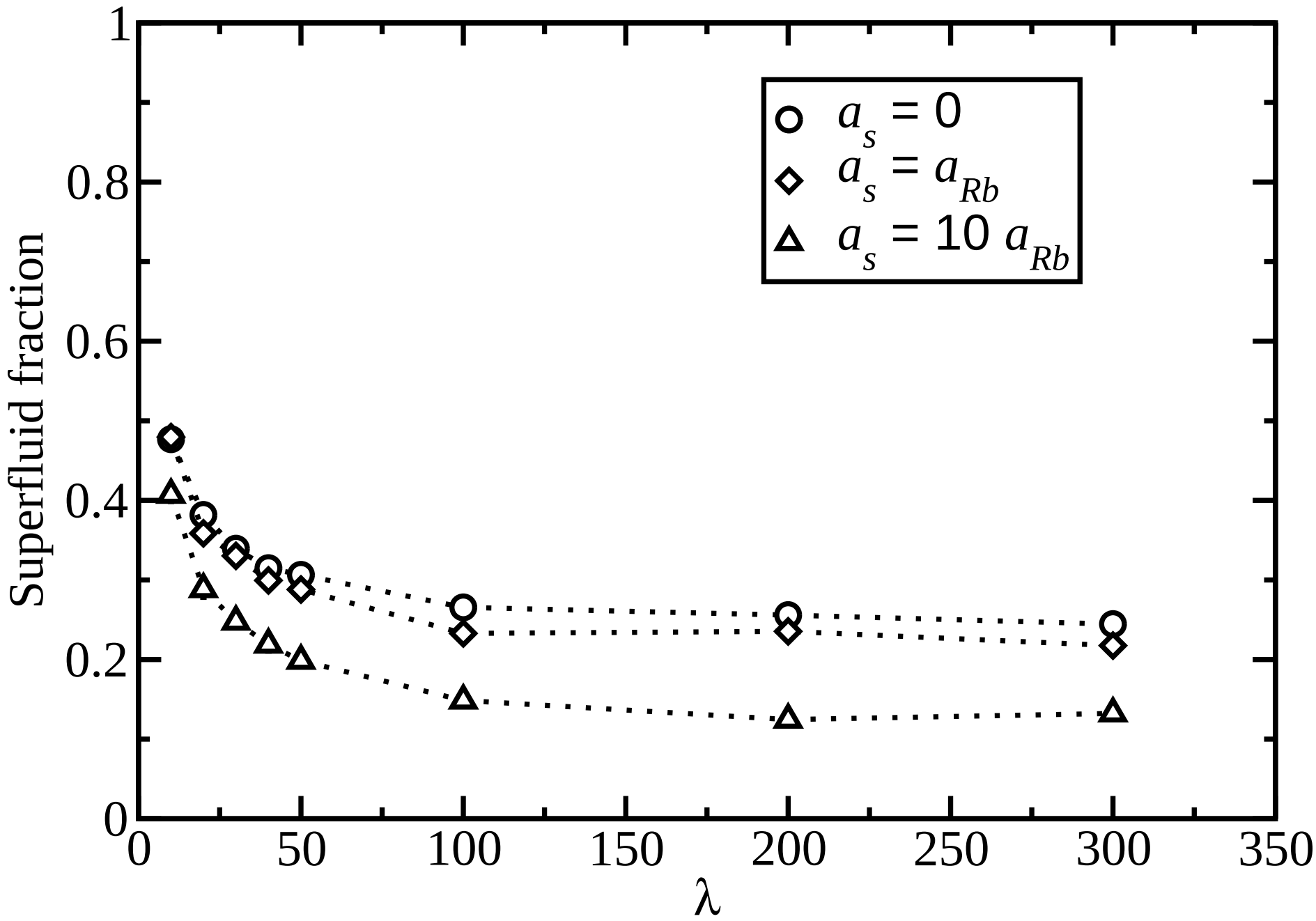
Superfluid fraction
λ
$a_s = 0$
$a_s = a_{Rb}$
$a_s = 10\ a_{Rb}$
0
0.2
0.4
0.6
0.8
1
0
50
100
150
200
250
300
350

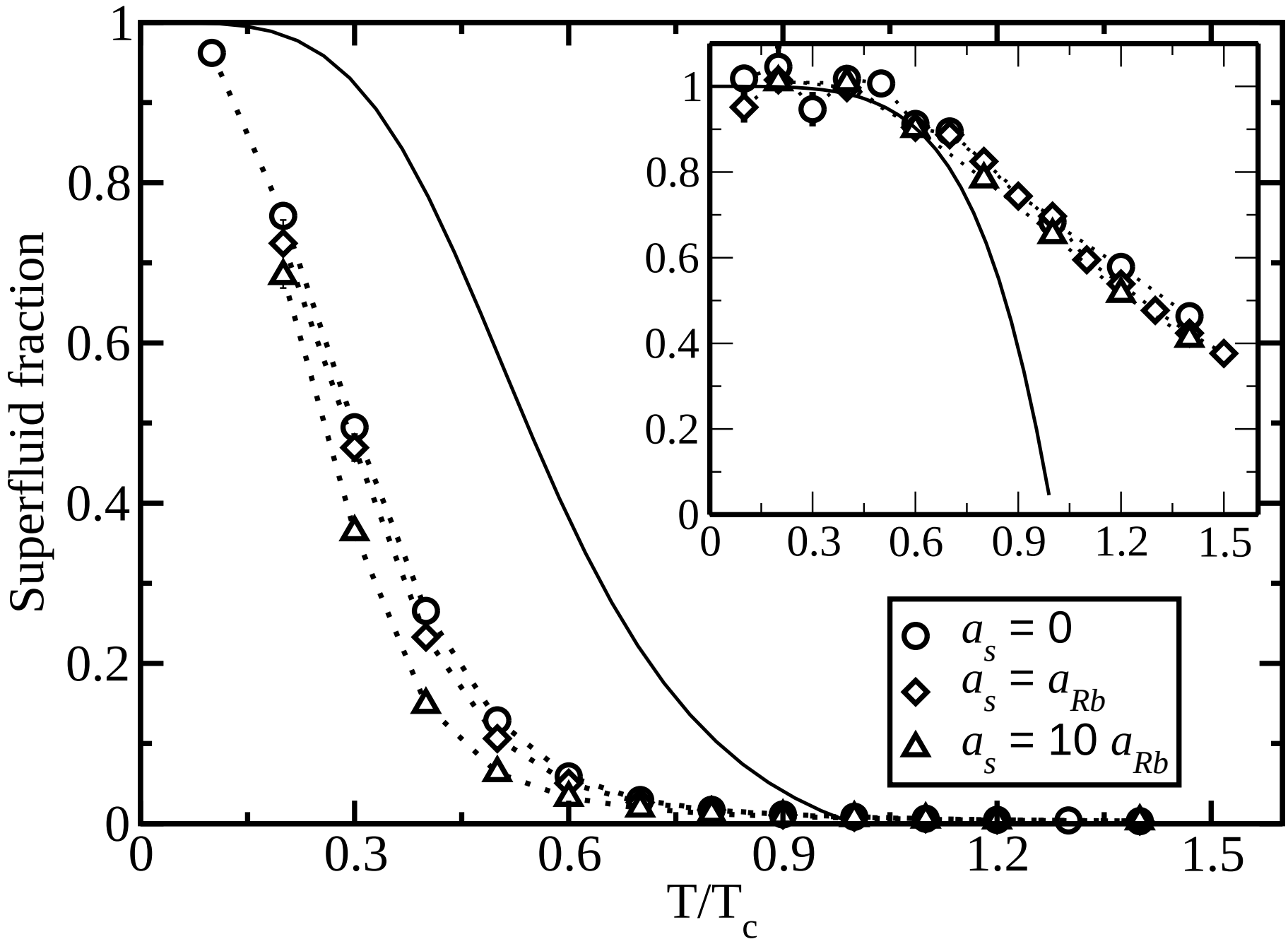
Superfluid fraction
T/T_c
0
0.2
0.4
0.6
0.8
1
0
0.3
0.6
0.9
1.2
1.5
a_s = 0
a_s = a_Rb
a_s = 10 a_Rb